Robotica: (2019) volume 37, pp. 2087–2103. © Cambridge University Press 2019
doi:10.1017/S0263574719000511

Optimizing Control of Passive Gait Training Exoskeleton Driven by Pneumatic Muscles Using Switch-Mode Firefly Algorithm

Yu Cao†, Jian Huang†*, Zhangbo Huang†, Xikai Tu‡ and Samer Mohammed¶

†*The Key Laboratory of Image Processing and Intelligent Control, School of Artificial Intelligence and Automation, Huazhong University of Science and Technology, Wuhan, China.*
E-mails: cao_yu@hust.edu.cn, huang_zb@hust.edu.cn
‡*School of Mechanical Engineering, Hubei University of Technology, Wuhan, China.*
E-mail: tuxikai@gmail.com
¶*The Laboratory of Images, Signals and Intelligent Systems (LISSI), University Paris-Est Créteil (UPEC), 94400 Vitry Sur Seine, France.*
E-mail: samer.mohammed@u-pec.fr

(Accepted March 18, 2019. First published online: April 22, 2019)

SUMMARY
This paper presents a lower-limb exoskeleton that is actuated by pneumatic muscle actuators (PMAs). This exoskeleton system is composed of the mechanical structures, a treadmill, and a weight support system. With the cooperative work of the three parts, the system aims to assist either the elderly for muscle strengthening by conducting walking activities or the stroke patients during a rehabilitation training program. A mechanism is developed to separate the PMAs from the wearer's legs to reduce the subject's physical exertion. Furthermore, considering the difficulty in the modeling of proposed PMAs-driven exoskeleton, a safe and model-free control strategy called proxy-based sliding mode control (PSMC) is used to ensure proper control of the exoskeleton. However, the favorable performances are strongly dependent on the appropriate control parameters, which may be difficult to obtain with blind tuning. Therefore, we propose a global parameters optimization algorithm called switch-mode firefly algorithm (SMFA) to automatically calculate the pre-defined object function and attain the most applicable parameters. Experimental studies are conducted, and the results show the effectiveness of the proposed method.

KEYWORDS: Lower-limb exoskeleton; Pneumatic muscle actuator; Proxy-based sliding-mode control; Switch-mode firefly algorithm.

1. Introduction

The aging problem is prominent all over the world. Full or partial losses of functions in the lower limbs caused by neurologic injuries have been continuously increasing in the elderly population,[1] which severely limit their daily abilities. With the development of the robotic technologies, robot-assisted therapy has shown great improvement for the overall rehabilitation processes.[2,3] However, most traditional rehabilitation robots are actuated by electric motors, which are usually expensive and lack of sufficient compliance. The pneumatic muscle actuators (PMAs) that are intrinsically soft and compliant have become promising actuators for the rehabilitation robots, in particular for

* Corresponding author. E-mail: huang_jan@mail.hust.edu.cn

https://doi.org/10.1017/S0263574719000511 Published online by Cambridge University Press

exoskeleton-based robotic devices. As a result, this type of soft actuating method has received widespread attention in recent years.[4–8] Teng et al.[9] proposed a low-cost, assisted knee-ankle-foot orthosis with PMAs for providing assistance during gait training. Cao et al.[10] developed a gait exoskeleton to simultaneously control the angular trajectory and compliance of the knee joint mechanism. Noting that during the human lower-limb motion, the rotation center of the knee joint will change, and its instantaneous trajectory is "J" type.[11] Currently, most rehabilitation exoskeletons rarely consider this structure of the human body. On the other hand, by comparison to electric motors, one should note the difficulty to achieve accurate control of the PMAs, due to the inherent features of high nonlinearities, hysteresis, and time-varying parameters. Therefore, accurate control of PMAs is still a challenging problem. Various control strategies have been developed to ensure satisfactory control performances, including adaptive control,[12,13] sliding-mode control (SMC),[14] dynamic surface control,[15] active model-based control,[16] active disturbance rejection control,[17] Proportion Integral Derivative (PID) control,[18] nonlinear predictive control,[19,20] so on. In general, such control algorithms mainly consider the dynamics of PMAs. Also, the dynamics of an multi-input multi-output (MIMO) robot system is complex and the control strategies often require accurate identification of the system's parameters.[21] These factors make it difficult for a PMAs-driven robot mechanism with complex dynamics to be satisfactorily controlled.

The proxy-based sliding-mode control (PSMC) firstly proposed by R. Kikuuwe is a safe extension of the traditional PID position control,[22,23] which is the combination of SMC and PID control. It is a model-free control strategy and as accurate as the PID control but is capable at the same time of slow, overdamped resuming motion without overshoots from large positional errors through parameter adjustment. It has been implemented in several applications, due to its favorable properties and easiness to be implemented. Gu et al.[24] applied robust tracking control of a piezoelectric-actuated nano-positioning stage composed of piezoelectric stack actuators and compliant flexure mechanisms. Damme et al.[25] presented a PSMC strategy on a two-degree-of-freedom (2-DOFs) planar manipulator actuated by the antagonistic configuration of PMAs. Prieto et al.[26] implemented the PSMC algorithm on a platform of 3-DOFs driven by PMAs with proportional flow valves. It is not an easy task to obtain satisfactory performance of the PSMC since there exist a few parameters to be tuned. The control parameters and the corresponding performance can be regarded as the input and output, respectively. Consequently, the tuning process can be regarded as an optimization problem, aiming to find the optimal control parameters, whereas, solving nonlinear optimization problems always faces several difficulties. Fortunately, nature-inspired metaheuristic algorithms are invented to solve such problems, including the genetic algorithm (GA),[27] the particle swarm optimization (PSO),[28] and the firefly algorithm (FA),[29] so on. Among them, the FA can find the global and local optima of the objective function simultaneously,[30] and it has been successfully applied in different fields.[31,32] However, the standard firefly algorithm (SFA) uses a fixed randomization parameter, which results in the slow convergence and might be trapped into local optima. In physical applications, the tuning process requires the control parameters to converge to a feasible solution quickly. Therefore, we proposed an improved FA algorithm called switch-mode firefly algorithm (SMFA), which firstly focuses on the exploration, and then switches to the exploitation. The exploration helps to quickly identify the promising region while the exploitation examines the promising regions more carefully to find a proper solution. Hence, the SMFA guarantees the quick convergence and a better feasible solution at the same time with the two-phase procedure.

The challenges of developing the PMAs-driven robotic exoskeleton for rehabilitation mainly come from two aspects. One is that the mechanical mechanism of the exoskeleton must conform to the human motion and fulfill various rehabilitation tasks, which require the leg orthoses to provide a sufficient range of motion and bandwidth. The other one is that the exoskeleton must be properly controlled to guarantee the effects of rehabilitative training and the safety of the patients, as well as comfort, simultaneously. This paper presents a novel PMAs-driven lower-limb exoskeleton system together with the optimization control of passive gait training based on SMFA. The main contribution of this paper lies in (1) the development of a novel PMAs-driven exoskeleton system for rehabilitation training, (2) a global parameters optimization solution for solving the problem of tuning the control parameters of the PSMC, and (3) the experimental studies for validating the proposed PMAs-driven exoskeleton system and the control strategy.

The rest of this paper is organized as follows. In Section 2, the mechanical structure of the exoskeleton and the control architecture are presented. In Section 3, the development of the control strategy is illustrated in detail. Then, in Section 4, the simulation studies are presented to evaluate

https://doi.org/10.1017/S0263574719000511 Published online by Cambridge University Press

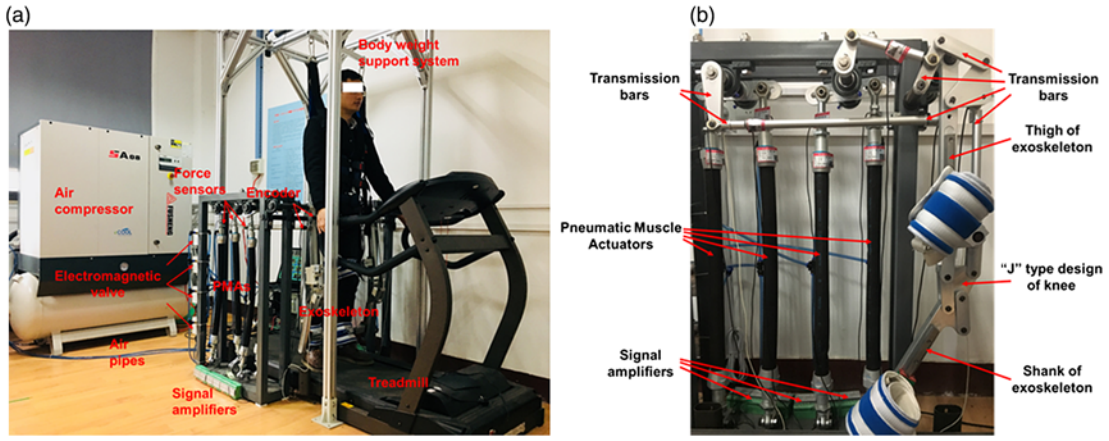


Fig. 1. (a) The physical exoskeleton system. (b) The structure of exoskeleton.

the SMFA and the control strategy of SMFA–PSMC. The experimental studies are conducted to demonstrate the effectiveness of the exoskeleton system for rehabilitation in Section 5. In Section 6, the conclusion is given.

2. PMAs-Driven Lower-Limb Exoskeleton

The whole lower-limb exoskeleton system is developed, as shown in Fig. 1. The overall system is comprised of three parts, including a body weight support (BWS) system, a treadmill, and a pair of PMAs-driven exoskeletons. When the patient is walking on the treadmill, the BWS system can assist the patient in maintaining balance. Meanwhile, the exoskeletons that interact with the user can provide necessary assistance and rehabilitative training to the movements of the legs, which are the most important portions of the whole system since their performances directly affect the rehabilitative effects and the interaction safety. Thus, the mechanism of the exoskeleton must conform to the laws of human motion and be intrinsically safe.

2.1. Design of PMAs-driven mechanical structure

2.1.1. Force transmission. The lower-limb exoskeleton system possesses two leg orthoses. Each of them has 2-DOFs, including the knee flexion/extension and hip flexion/extension. The rotational joint is driven by the antagonistic configuration of PMAs since a single PMA can only provide unidirectional actuation. An antagonistic configuration of PMAs is controlled by

$$\begin{cases} P_a = P_{0a} + \Delta P \\ P_b = P_{0b} - \Delta P, \end{cases} \tag{1}$$

where P_a, P_b are the input pressures of the antagonistic PMAs, respectively. P_{0a}, P_{0b} represent the nominal inner pressures of the PMAs. ΔP denotes the increment of the inner pressure. As a result, one PMA in an antagonistic pair will inflate and produce a force F_a. The other one will deflate and produce a smaller force F_b in the same direction. Then, a rotational torque is generated at point R. As a result, an antagonistic configuration of PMAs can provide a rotational torque for one rotational joint, just like a motor. Consequently, when the point R in Fig. 2(a) is fixed at point A or B of Fig. 2(b), the rotational moment τ can be provided to the point A or B and drives the mechanism.

The two PMAs-driven leg orthoses are symmetrical and powered by eight PMAs that consist of four groups of antagonistic PMAs. Thus, one leg requires two groups of antagonistic PMAs to provide the rotational torques τ_h, τ_k for the hip and knee joints.

To facilitate the presentation, some notations describing the mechanical structure should be clarified first, as shown in Fig. 2(b):

- A, B, C, D – anchored points on the fixed frame.
- F, G – the angle encoders mounting points.
- E – the point where the triangle block is fixed on the thigh exoskeleton.
- l_1 – length of thigh exoskeleton.
- l_2 – length of calf exoskeleton.

https://doi.org/10.1017/S0263574719000511 Published online by Cambridge University Press

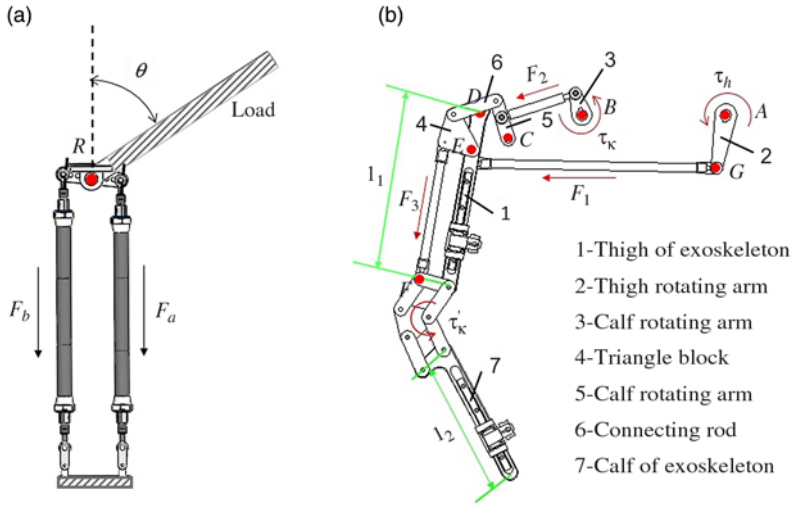


Fig. 2. The force transmission of the leg orthosis.

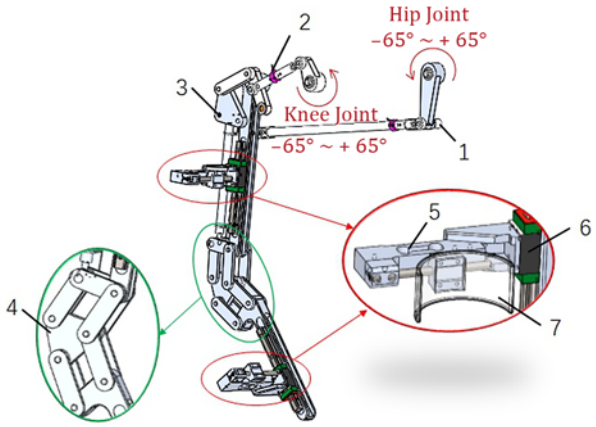


Fig. 3. The mechanical structure of the leg orthosis. 1 – Hip joint angle encoder, 2 – Force sensor, 3 – Knee joint angle encoder, 4 – "J"-type rotational center, 5 – Cantilever beam sensor, 6 – Sliding block, 7 – Elastic strap.

When a driving torque τ_h acts on point A, a force F_1 will be generated. Since points A, D are anchored on a fixed frame, the rotation angle of thigh exoskeleton around point D will be the same as the rotation angle of thigh rotating arm around the point A. This is because they are like two fixed points in a parallelogram. And the amount of rotation can be regarded as the hip angle θ_1.

Similarly, when a driving torque τ_k acts on point B, the rotation angle of calf rotating arm around the point C will be the same as the rotation angle of another calf rotating arm around the point B. Also, a quadrangle can be formed with the fixed point C, E, the connecting rod, and one side of the triangle block. When the calf rotating arm rotates around point C, the triangle block will rotate around point E correspondingly. The increments of the rotation angle are not the same since this is not a parallelogram. Then, a force F_3 is generated, and it results in a driving torque τ_k' applied to the knee joint, by which the knee joint angle θ_2 is generated. Specifically, two angle encoders are installed at the points G and F to measure the rotational angles θ_1 and θ_2 of hip and knee joints, respectively.

2.1.2. Design for fitting lower-limb motion. At present, the design of the exoskeleton mainly has two problems: (a) the poor fitting leg movement of walking *that may cause discomfort, pain, and increased risk of injury and occlusion*[33]; (b) the rotation of the knee joint is not simply rotated around a fixed point, and the instantaneous trajectory is "J"-type.[11] Based on the above analysis, we propose several improvements for the mechanical structure, as shown in Fig. 3. It is shown that there exist

https://doi.org/10.1017/S0263574719000511 Published online by Cambridge University Press

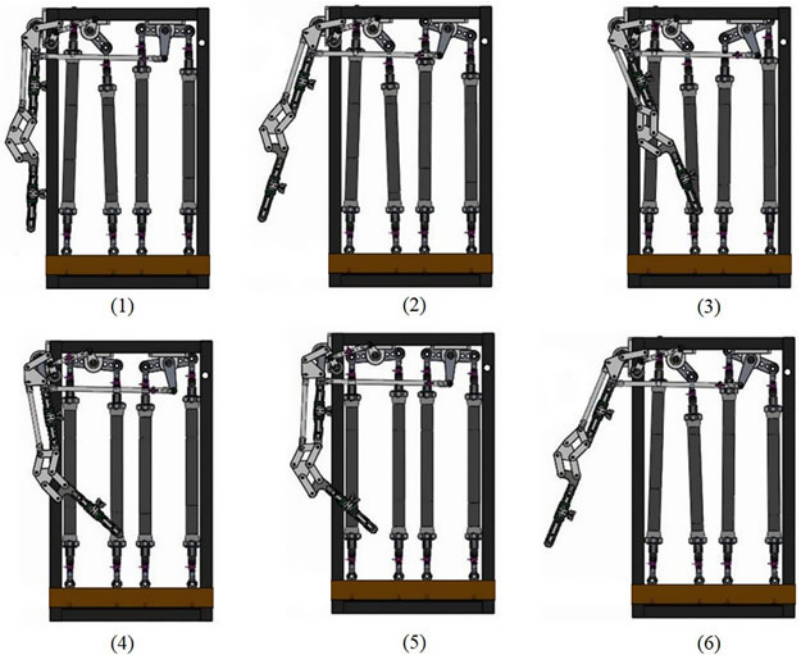


Fig. 4. The gait movement of a leg orthosis. (1) Initial swing, (2) initial contact, (3) terminal stance, (4) pre-swing, (5) mid swing, (6) terminal swing.

two sliding blocks on the thigh and shank, together with bases and corresponding cantilever beam sensors. The human leg is tied by elastic straps. When the patients wear the exoskeleton for walking training, the sliding blocks slide up and down to fit the lower-limb motion. Similarly, adjusting the position of the slider also makes the exoskeleton to fit people of different heights. Also, the interaction between the human and the exoskeleton can be measured with the cantilever beam sensors. During the human movement, the rotation center of the knee joint will change. Hence, an anthropomorphic design of knee joint is presented. Two parallelograms are constructed with a triangular block. This design increases the freedom of rotation at the knee joint.

2.1.3. Movement of leg orthosis. The installation of the angle encoders and force sensors are presented in Fig. 3. The rotations of the hip and knee joint are based on the two groups of the antagonistic PMAs. Therefore, one leg orthosis can be regarded as a system of two inputs, ΔP_h and ΔP_k, and two outputs θ_1 and θ_2. The movement of the leg orthosis is shown in Fig. 4. Figure 4 denotes the different states of the joints rotation that depends on the contraction of PMAs, including the overall process of a human gait cycle. With this mechanical design, the two joints can be controlled independently, which brings great convenience to our applications.

2.2. Control architecture

The structure of the proposed exoskeleton system is illustrated in Fig. 5. The development of the control architecture is basically comprised of the following components: (1) the exoskeleton, angle encoders (Omron, E6A2-CWZ3E), pressure sensors (Bongshin, CDFSC), electromagnetic valves (Festo, VPPM), (2) the data acquisition/control layer, which mainly serves two functions (one is collecting the real-time sensory data of the exoskeleton system and sending to the computer via the signal acquisition card (PCI-NI 6229), and the other is sending the control signals to the electromagnetic valves to adjust the inner pressure of the PMAs), and (3) control computers, which are responsible for executing the algorithms in real time to obtain the control signals and send them to the data acquisition/control layer.

The setup of the system is based on the xPC target, a product from MathWorks. This environment provides mathematically complex control strategies with the dedicated hardware by SIMULINK/BLOCKS. Two computers are utilized, which serve as the host and the target, respectively. The host computer is installed with MATLAB/SIMULINK, C/C++ compiler and applies models to generate executable codes, while the target computer executes the code in real time. They

https://doi.org/10.1017/S0263574719000511 Published online by Cambridge University Press

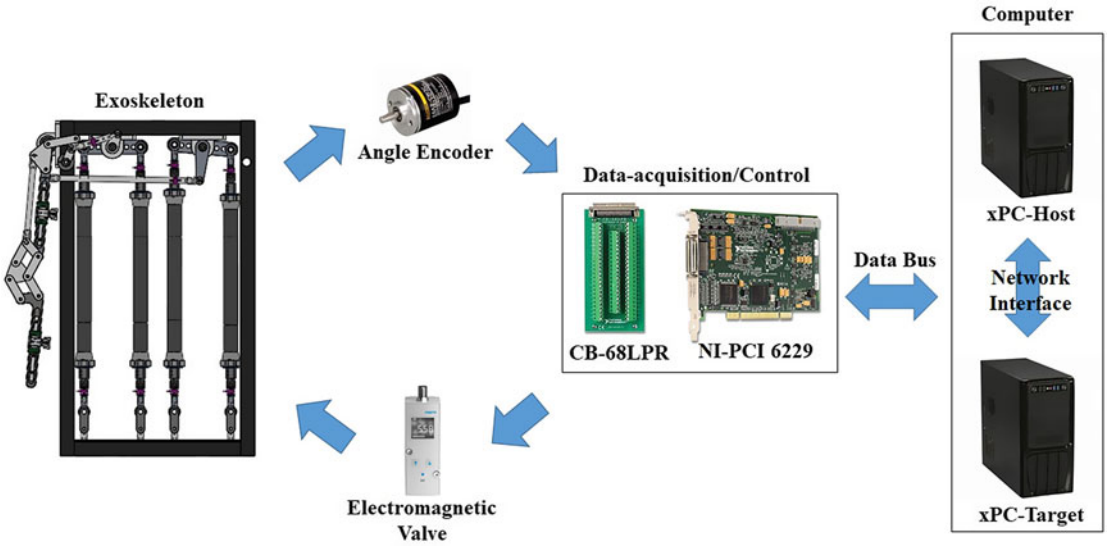


Fig. 5. The control architecture of the exoskeleton system.

are connected via a network interface. Hence, the xPC target can provide the necessary software that makes use of real-time resources on the target computer hardware.

This approach focuses on the passive training mode of the exoskeleton system that can assist the patients. This enables the exoskeleton leg to track continuous desired trajectories, especially the normal human gait.

3. Controller Design

There exist multiple closed chains in the mechanical structure of the PMAs-driven leg orthosis which makes the dynamics of the exoskeleton extremely complex. Furthermore, the dynamics of PMAs possesses features of strong nonlinearities, time-varying parameters, and uncertainties. In considering the above reasons, it is quite difficult to model the exoskeleton accurately. Therefore, a model-free control strategy might be more suitable for controlling the exoskeleton. However, model-free control strategies, for example, the PID control, usually require the appropriate parameters. The tuning rules are strongly dependent on the experience, and it is often difficult to obtain optimal values. Therefore, we would like to propose a model-free control strategy with online tuning the control parameters to realize the automatic parameter tuning.

3.1. Proxy-based sliding mode control[23]

The PSMC is a model-free position control that is as accurate as conventional PID control but is capable of slow, overdamped resuming motion without overshoots from large positional errors. Its properties indicate that the strategy is a safe extension of PID position control.

The principle of PSMC is illustrated in Fig. 6. The object is connected to a virtual object, which is called a proxy, using a PID-type virtual coupling. The PID controller causes an interaction force f_{pid}, while the proxy is controlled by an SMC that produces a force f_{smc} to make the proxy track the desired trajectory.

Let $x, x_p, x_d \in \Re$ denote the positions of the controlled object, the proxy, and the desired trajectory. The force $f_{pid} \in \Re$ produced by the PID-type virtual coupling can be written as follows:

$$f_{pid} = k_p \dot{a} + k_i a + k_d \ddot{a}, \tag{2}$$

with

$$a = \int (x_p - x) dt,$$

where k_p, k_i, and k_d are positive real numbers, which are the proportional, integral, and derivative gains, respectively. These parameters should be appropriately tuned.

https://doi.org/10.1017/S0263574719000511 Published online by Cambridge University Press

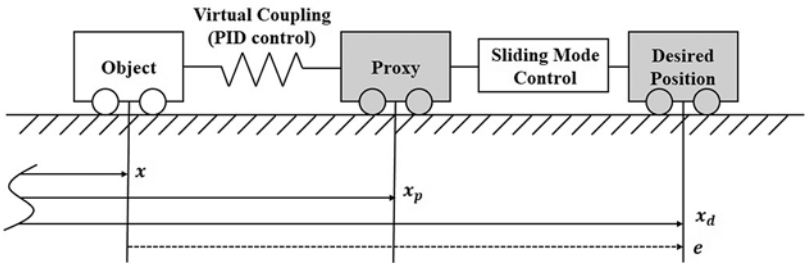


Fig. 6. The principle of the PSMC. Through a virtual object called "proxy," the controlled object does not track the desired trajectory directly.

On the other hand, we define two sliding manifolds with a positive constant λ:

$$\sigma_1 = x_d - x_p + \lambda(\dot{x}_d - \dot{x}_p), \tag{3}$$

$$\sigma_2 = x_d - x + \lambda(\dot{x}_d - \dot{x}). \tag{4}$$

Then, the SMC law that is applied to the proxy is given by

$$f_{smc} = F\mathrm{sgn}(\sigma_1), \tag{5}$$

where $F > 0$ denotes the force limit and should be chosen by considering the tradeoff between the control performance and the safety.

Hence, the motion of the proxy can be governed by

$$m\ddot{x}_p = f_{smc} - f_{pid} \tag{6}$$

where m is mass of the proxy. Let $m = 0$, then the controller output $f = f_{pid} = f_{smc}$, and the overall formation of the PSMC can be written as

$$\begin{cases} \ddot{a} = -\dfrac{k_p\dot{a} + k_i a}{k_d} + \dfrac{F}{k_d} sat\left(\dfrac{k_d}{F}\left(\dfrac{\sigma_2 - \dot{a}}{\lambda} + \dfrac{k_p\dot{a} + k_i a}{k_d}\right)\right) \\ f = F sat\left(\dfrac{k_d}{F}\left(\dfrac{\sigma_2 - \dot{a}}{\lambda} + \dfrac{k_p\dot{a} + k_i a}{k_d}\right)\right) \end{cases} \tag{7}$$

with

$$sat(y) = \begin{cases} \mathrm{sgn}(y), & if \quad |y| > 1 \\ y, & if \quad |y| \le 1. \end{cases}$$

3.2. Optimization control of passive gait training

The properly tuned parameters k_p, k_i, k_d, λ of PSMC are required to get one joint of the exoskeleton controlled. Also, an antagonistic configuration of PMAs actuates one joint, referring to (1), and the nominal inner pressures P_{0a}, P_{0b} of the PMAs should be suitably determined. Here we assume that $P_0 = P_{0a} = P_{0b}$. Hence, there are five parameters to be adjusted for one joint of the exoskeleton, whereas it is difficult to adjust these parameters at the same time. In this situation, an optimization method called FA is applied to adjust these parameters automatically.

The FA is a biologically inspired algorithm.[29] It can find global optima as well as all the local optima simultaneously in a very effective manner, and it uses the following three simplifying assumptions:

- All fireflies are unisex and are attracted to each other.
- The attractiveness is proportional to the brightness of a firefly and is inversely proportional to the distance, which means that the less bright firefly will move toward the brighter one. The brightest firefly moves randomly since there are no other brighter fireflies to attract it.
- The brightness of a firefly is determined by the objective function.

https://doi.org/10.1017/S0263574719000511 Published online by Cambridge University Press

To obtain the most appropriate parameters of the PSMC for attaining the best control performance of the exoskeleton system, the objective function is firstly defined to specify the brightness of the firefly:

$$g(\mathbf{s}_j) = \mu \frac{1}{N} \sum_{t=1}^{N} |x_d(t) - x(t)| + \nu \max_{t \in [1,N]} |x_d(t) - x(t)|, \tag{8}$$

where x, x_d denote the rotational angle and the desired angle of one joint. N is the total sampling number. μ, ν are positive constants. $\mathbf{s}_j = [k_p, k_i, k_d, \lambda, P_0]^T$ presents a vector of the pending parameters. The objective function is the weighted sum of the average error and the maximum error. Selecting values of μ, ν, the objective function can be more biased toward the maximum error or average error. Hence, when the value of the objective function is smaller, the control effect is better. Therefore, the smaller $g(\mathbf{s}_j)$ is, the brighter $\mathbf{s}_j$ is.

As we know, the average error and maximum error can describe the tracking performance from two different perspectives. The weights of them directly determine the values of the objective function. When the average error is ignored, the object function has few ways to take care of the overall control performance. On the contrary, when the maximum error is ignored, there may occur a big overshoot, which results in an unsafe situation for the exoskeleton. Therefore, we would like to reduce both of them simultaneously. However, we have to make a compromise on these two factors. As far as our concern, we have to guarantee the global effectiveness of the control performance. Thus the weight would be more biased toward the average error. Meanwhile, we want to reduce the maximum error as much as possible. Several sets of μ, ν have to be chosen to test each performance. Finally, the values of μ, ν are set as 0.7 and 0.3, respectively.

On the other hand, the attractiveness is relative, since it is judged by other fireflies. Thus, the attractiveness varies with the distance r_{ij} between firefly $\mathbf{s}_i$ and firefly $\mathbf{s}_j$:

$$r_{ij} = ||\mathbf{s}_i - \mathbf{s}_j|| = \sqrt{(\mathbf{s}_i - \mathbf{s}_j)^T (\mathbf{s}_i - \mathbf{s}_j)}. \tag{9}$$

The attractiveness function $\beta(r_{ij})$ is monotonically decreasing, and it can be expressed as

$$\beta(r_{ij}) = \beta_0 e^{-\gamma r_{ij}^2}, \tag{10}$$

where β_0 is the attractiveness at $r_{ij} = 0$ and γ is a fixed value that relates to the length scale in the optimization problem.

When a firefly i is attracted to another more brighter firefly j, the movement of i will be generated and determined by

$$\mathbf{s}_{i,k} = \mathbf{s}_{i,k} + \beta_0 e^{-\gamma r_{ij}^2} (\mathbf{s}_{j,k} - \mathbf{s}_{i,k}) + \alpha \varepsilon, \tag{11}$$

where $\mathbf{s}_{i,k}$ denotes the kth element in $\mathbf{s}_i$ and ε is a random value usually uniformly distributed in $[-0.5, 0.5]$.

The proposed SMFA starts with exploration by using a fixed randomization parameter α, just like SFA. After several iterations, when the exploration has difficulty improving the performance among all the fireflies, we should switch from exploration to exploitation. Therefore, the switching condition is significant. Let $g_k = \min_{i=1,\ldots,n} g(\mathbf{s}_i)$ be the best fitness in the kth iteration. Then the changing rate of g_k can be denoted as

$$\dot{g}_k = \frac{g_k - g_{k-1}}{g_{k-1} - g_{k-2}}. \tag{12}$$

If the changing rate $\dot{g}_k$ is smaller than a pre-defined threshold ξ, it means that the firefly has reached a near-optimal value. And it is the time for switching. However, it may be difficult to find a suitable ξ as a priori, so we define a maximum number of exploration K_0 and force the SMFA to switch to exploitation after K_0 iterations.

On the other hand, the randomization plays an important role in FA, since it increases the diversity of the firefly population. The large randomization parameter α enables the FA to explore the search

https://doi.org/10.1017/S0263574719000511 Published online by Cambridge University Press

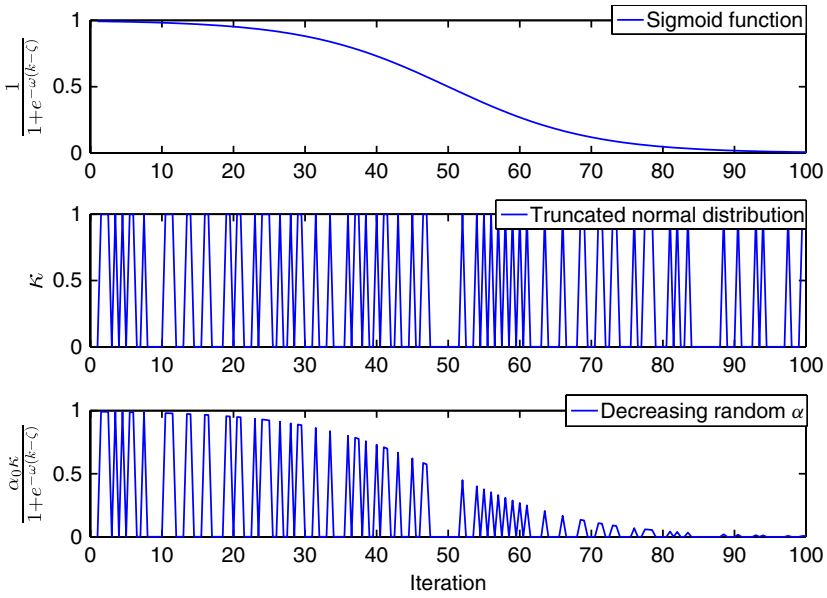


Fig. 7. The gradually decreasing random α, which consists of two parts. One is the gradually decreasing part, referring to the sigmoid function, and the other one is a truncated normal distribution. *The corresponding parameters are set as* $\alpha_0 = 1$, $\omega = -0.1$, $\zeta = 50$.

space more quickly, but it leads to slow convergence in exploitation. To deal with this problem, we proposed a gradually decreasing random α for the exploitation mode of the SMFA:

$$\alpha = \frac{\kappa \alpha_0}{1 + e^{-\omega(k-\zeta)}}, \tag{13}$$

where α_0 is the randomization parameter in exploration. κ that follows $\kappa \sim N(0.5, 1)$ in $(0, 1)$ is a random number from a truncated normal distribution.[34] ζ is a constant that is often set as half of the maximum iterations, while ω can be determined according to the requirement of convergence speed. k is the current iteration number.

To better describe α, the definitions of exploration and exploitation should be emphasized[35]: (1) Exploration, which probes the entire search space with the hope of finding all promising regions. Its goal is to diversify the search to avoid getting trapped in a local optimum. (2) Exploitation, which probes a local region of the search space with the hope of improving a promising solution that has already been identified through exploration.

The randomization parameter α is the coefficient of the random movement of a firefly, which influences both the exploration and exploitation processes. In the exploration process, the value of α should be relatively large, since this enables fireflies to explore the entire searching space more quickly. In the exploitation process, the value of α should be relatively small, which results in the fireflies searching the promising region more carefully to improve the performance. The SFA used a fixed randomization parameter.[36] Even though it can explore the search space quickly in the exploration, it is difficult to be convergent in exploitation. Based on the above consideration, a decreasing α should be used, which has been appeared in ref. [36] called the simulated strategy firefly algorithm (SAFA). However, this may lead the algorithm to trap into a local optimum, because the value of α may become too small for further exploration when the exploration process is not over.

Therefore, we propose an SMFA, which firstly utilizes a fixed randomization parameter in exploration and uses a gradually decreasing random randomization parameter in exploitation. The randomization parameter α takes effect in exploitation which consists of two parts. One is the gradually decreasing part, referring to the sigmoid function, and the other one is a truncated normal distribution, which can increase the randomness of α. In this way, the algorithm can meet the requirement of exploration and exploitation, simultaneously.

The typical example of α is shown in Fig. 7. It is clear that as the iteration k increases, α is a gradually decreasing random number, which enables the SMFA to focus on the exploitation.

https://doi.org/10.1017/S0263574719000511 Published online by Cambridge University Press

4. Simulation Studies

In this section, the proposed SMFA–PSMC strategy is applied to control the lower-limb exoskeleton system. A healthy subject's knee and hip joint trajectories during level walking are adopted as the reference in this paper. A comfortable walking speed (15.9 steps/min) is selected according to ref.[37] Based on that, we slowed down the walking speed a little bit to ensure experimental safety. Therefore, we choose the walking speed as 12 steps/min. Several optimization algorithms are used for comparisons, including the SFA, the SAFA, and the SMFA to show the evaluation of the proposed method. All the algorithm developments are conducted with MATLAB, version 2013b, installed on a computer with a clock speed of 3.6 GHz and 8 GB RAM, in a Microsoft Windows 10 environment.

Algorithm 1 SMFA–PSMC

Require: $g(\mathbf{s})$, the object function to be minimize;
n, the size of the firefly population;
α_0, the initial randomization parameter;
β_0, the maximum value of attractiveness;
γ, the light absorption coefficient;
K, the maximum number of iterations;
K_0, the maximum number of exploration;
Ensure: $\mathbf{s}^*$, which minimizes $g(\mathbf{s})$;

```
Generate initial population of fireflies {s_i}_{i=1,..,n};
while k < K do
    for i = 1 to n do
        Apply s_i to PSMC for the physical system;
        Wait for the physical experiment done;
        Obtain the experimental results;
        Compute g(s_i) based on (8);
    end for
    if ġ_k > ξ and k ≤ K_0 then
        α = α_0;
    else
        Compute α by (13);
    end if
    for i = 1 to n do
        for j = 1 to n do
            if g(s_i) > g(s_j) then
                Compute r_ij, according to (9);
                Move firefly i towards j according to (11)
            end if
        end for
    end for
    Rank the fireflies and find the current best;
end while
Return s* = arg min_{i=1,..,n} g(s_i)
```

4.1. System modeling

The modeling of the PMAs-driven leg orthosis should include both the dynamics of the PMAs and the mechanical structure. The antagonistic configurations of PMAs provide the driving torques, whereas, due to the strong nonlinearities and the uncertainties of PMAs, as well as the complexity of the mechanical structure, it is difficult to model the whole system accurately. Therefore, we ignore all the frictions and simplify the mechanical structure as two-connecting bars. Then, the dynamics of the exoskeleton can be presented based on the Lagrangian Function:

$$\mathbf{M}(\mathbf{q})\ddot{\mathbf{q}} + \mathbf{N}(\mathbf{q}, \dot{\mathbf{q}}) = \boldsymbol{\tau}_0 + \mathbf{G}\Delta\mathbf{P}, \tag{14}$$

https://doi.org/10.1017/S0263574719000511 Published online by Cambridge University Press

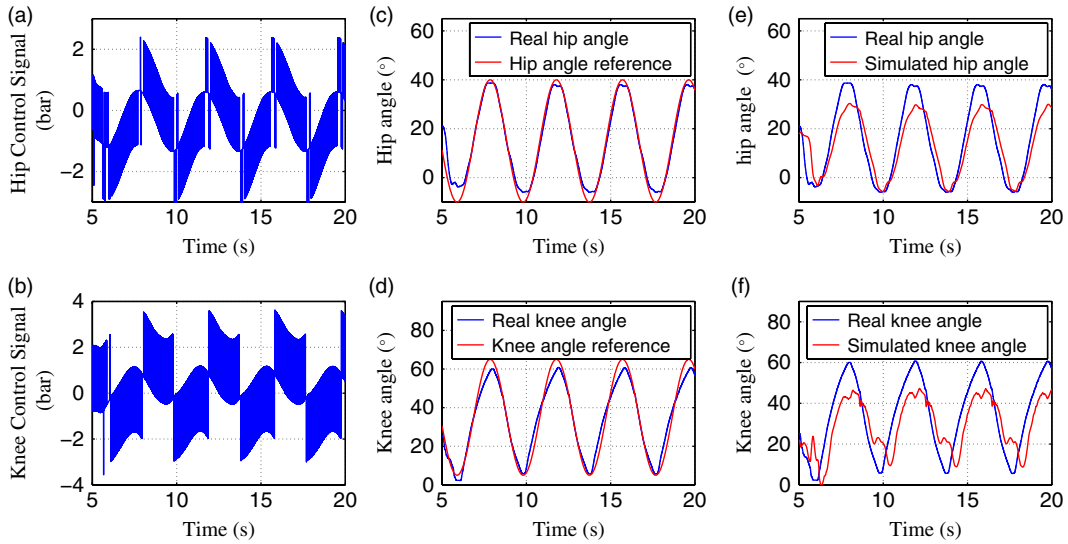


Fig. 8. From left to right, the figures are the control signals of hip and knee joints; control performance of the real joints based on PSMC; the comparisons between the simulated joint angles and the real joint angles.

where $\mathbf{q} = [\theta_1, \theta_2]$, $\mathbf{M}(\mathbf{q})$ is a 2×2 inertia matrix of the exoskeleton leg. $\mathbf{N}(\mathbf{q}, \dot{\mathbf{q}})$ is a vector related to $\mathbf{q}$, $\dot{\mathbf{q}}$ and

$$\boldsymbol{\tau}_0 = [\, \tau_{h0} \;\; \tau_{k0} \,]^T, \; \Delta\mathbf{P} = [\, \Delta P_h \;\; \Delta P_k \,]^T, \; \mathbf{G} = \begin{bmatrix} \tau_{h1} & 0 \\ 0 & \tau_{k1} \end{bmatrix},$$

where τ_{h0}, τ_{k0}, τ_{h1}, τ_{k1} are the input torques of hip and knee joint produced by antagonistic configurations of PMAs. ΔP_h and ΔP_k are the control signals of the hip and knee joints, respectively. Although it is an approximate model, it still can make sense. The comparisons of the approximate model and the actual system are shown in Fig. 8.

The control signals of the hip and knee joints come from the PSMC with sinusoidal reference trajectories, referring to Fig. 8(a) and (b). The tracking performance of the hip and knee joints are shown in Fig. 8(c) and (d), respectively. The angular outputs of exoskeleton joints track the reference trajectory with favorable accuracy. Outputs are presented by red trajectories in Fig. 8(e) and (f) by inputting the control signals in Fig. 8(a) and (b) into the dynamic model of the exoskeleton. The overall processes are illustrated as follows: (1) We firstly give out a sinusoidal reference trajectory and apply PSMC to calculate the control signals with this reference for the physical exoskeleton. Figure 8(a) and (b) shows the corresponding control signals, and Fig. 8(c) and (d) shows the performance of the physical exoskeleton. (2) By applying the previously calculated control signals to the dynamical simulation model, a performance of the simulated model can be obtained. Then, we compare the results of the simulated model and the actual output of the physical exoskeleton, as shown in Fig. 8(e) and (f). Although there are some differences between the simulation system model and the actual system, the results show that the simulated model is similar to the physical exoskeleton system. And the PSMC is a kind of model-free control strategy, which is suitable for both the simulation system model and the actual model.

4.2. Simulation results

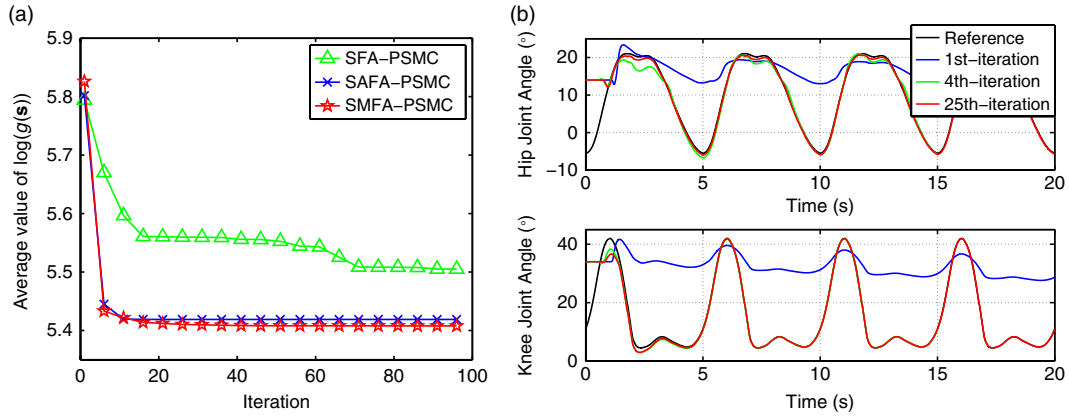
Since this application aims at passive training for the patients, the reference trajectory is the human gait rather than a sinusoidal function. Under this condition, we intend to provide a guidance for the adjustment of the control strategy in the actual system based on the results of the simulation. Several algorithms, including the SFA–PSMC, SAFA–PSMC, and SMFA–PSMC are used to show the superiority of the proposed strategy.

On the other hand, the nature-inspired metaheuristic algorithms are dependent on a certain degree of randomness. We run the program for 40 times to eliminate the effects of randomness. The average

https://doi.org/10.1017/S0263574719000511 Published online by Cambridge University Press

Table I. The tracking performance of the SMFA–PSMC strategies in different iterations.

Iteration	**Hip angle of $g(\mathbf{s})$**	**Knee angle of $g(\mathbf{s})$**
First iteration	11.0066	21.4182
Fourth iteration	7.0512	7.6208
Twenty fifth iteration	6.5397	7.4542



The performance of the PSMC with FA-based strategies.

The tracking performance of the SMFA-PSMC strategies.

Fig. 9. The performance of the proposed strategies.

value of $\log(g(\mathbf{s}))$ in each iteration is presented in Fig. 9(a). It is shown that all the FA-based algorithms regulate the control parameters. The convergence of the algorithms is quite different. After 60 iterations, the SFA–PSMC gradually converges, and the tracking performance is the worst among the three strategies because of the bigger value of $g(\mathbf{s})$. The average values of $g(\mathbf{s})$ of the SAFA–PSMC and SMFA–PSMC decrease quickly in the first five iterations. After 25 iterations, the value of $g(\mathbf{s})$ has not changed anymore, indicating that the SMFA–PSMC examines the promising regions more carefully and it has found the best solution in the region.

The tracking performance of the hip and knee joints is shown in Fig. 9(b). The tracking errors become smaller as the iteration increases. The value of $g(\mathbf{s})$ is quite small after five iterations. In the subsequent iterations, the tracking errors do not decrease significantly, since the strategy searches for the solution in a small promising region, as shown in Table I.

5. Experimental Studies

5.1. Experiment setup

In terms of the control strategy implementation, the SIMULATION/MODEL that carries PSMC algorithm is compiled into binary files and downloaded to the target computer, which is reusable in the xPC target environment. The sampling frequency is 1 kHz. The platform is comprised of electromagnetic valves, signal amplifiers, PMAs, angle encoders, force sensors, a data acquisition board, leg orthoses, an air compressor, a treadmill, and a BWS system, as shown in Fig. 1(a). Their parameters are presented in Table II.

In general, the FA algorithm requires a certain number of firefly populations n, and the optimization process needs multiple iterations n_i. Also, calculating the brightness of a firefly costs a number of total sampling time T. Let N be the total sampling number. The entire optimization time is $n \times n_i \times N \times T$. Actually, this takes a long time for obtaining the optimal control parameters, which causes difficulties for human training of achieving long-term wearable exoskeleton training optimization. Hence, we use the load to simulate the human leg weight and then optimize the control parameters. The weight of the load is determined by the body segment inertial parameters (BSIPs), which is interested in the mass, the center of mass (CoM), the location, and the moment of inertia of body segments.[38] The related work can be found in refs.[39–41] In this paper, the mounted loads on

https://doi.org/10.1017/S0263574719000511 Published online by Cambridge University Press

Table II. The main devices.

Name	Type	Performance
Electromagnetic valve	Festo, VPPM-6L	Input: 0–10 V Output: 0–1.1 Mpa
Data acquisition board	NI PCI-6229	32 AI and 4 AO 48 digital I/O buses Sampling rate: 250 kS/s
Force sensor	Bongshin, CDFS	Measurement range: 0–200 kg Sensitivity: 2 ± 0.1 mV/V Accuracy: $0.03\%F \cdot S$ Supply voltage: 10 VDC
Power supply	Q-120DE	Input: AC 220 10%50 Hz Output: ±5, ±12, ±24 V
Pneumatic muscle	FESTO, MAS-40-400N	Inner diameter: 40 mm Rated length: 120–9000 mm Lifting force: 0–6000 N
Angle encoder	OMRON, E6A2-CWZ3E	Resolution: 1000 P/R Input: 5–12 V
Air compressor	FUSHENG, SA08	Capacity: 270 L Power: 800 W Exhaust pressure: 0.8 MPa
Signal amplifier	PT350C	Input: 0–10 V DC Output: 0–5 V
Treadmill	American Motion Fitness	Velocity: 0.1–10 km/h Running area: 495 × 1540 mm

the thigh and calf are selected as 6.5 and 4.0 kg, respectively. The control parameters are optimized to obtain the best control performance by calculating the object function, referring to (8). The upper bound and the lower bound of the control parameters are selected, and the fireflies can converge with a few of iterations and find the optimal control parameters in this range.

5.2. Experimental results

Figure 10(a) presents the convergence procedure of the SMFA with the object function of joints. Since each firefly represents a set of control parameters, we collected all the control parameters $\mathbf{S} = [\mathbf{s}_1, \mathbf{s}_2, \ldots, \mathbf{s}_n]$ during the convergence of firefly and normalize them according to

$$\mathbf{S}' = \frac{\mathbf{S} - \max(\mathbf{S})}{\max(\mathbf{S}) - \min(\mathbf{S})}. \tag{15}$$

It is clear that fireflies are randomly distributed within a range in the beginning. All fireflies have converged to a very small range after 25th iteration. Because of the actual implementation, it is impossible to make every experiment exactly the same. Therefore, when fireflies converge within a certain small range, it is considered that the current optimal control parameter is obtained, as shown in Fig. 10(b).

The tracking performances of hip and knee joints are presented in Fig. 11. After the 25th iteration, the control error has been greatly reduced, and the control effect has been improved. Therefore, the physical exoskeleton system can be properly controlled based on this control strategy.

In the following part, several experiments were conducted with seven healthy volunteer subjects, as shown in Table III, to further investigate the potential of applying the SMFA–PSMC in robotic gait rehabilitation training. The subjects were healthy and had no lower-limb injury. The subjects were requested to fully relax their lower limb and let the mechanism to guide the movement of the

https://doi.org/10.1017/S0263574719000511 Published online by Cambridge University Press

Table III. The information of the healthy subjects and the tracking performance with RMSE.

Subject	**Age**	**Sex**	**Height (cm)**	**Weight (kg)**	**Hip joint (°)**	**Knee joint (°)**
S1	Male	29	168	60	2.458	1.339
S2	Male	23	169.5	75	2.660	1.270
S3	Male	24	165	57	2.229	1.298
S4	Male	25	169.5	63	2.307	1.275
S5	Male	23	176	68	2.4682	1.3104
S6	Female	21	158	43	2.3731	1.3555
S7	Male	40	175	73.5	2.7741	1.4188

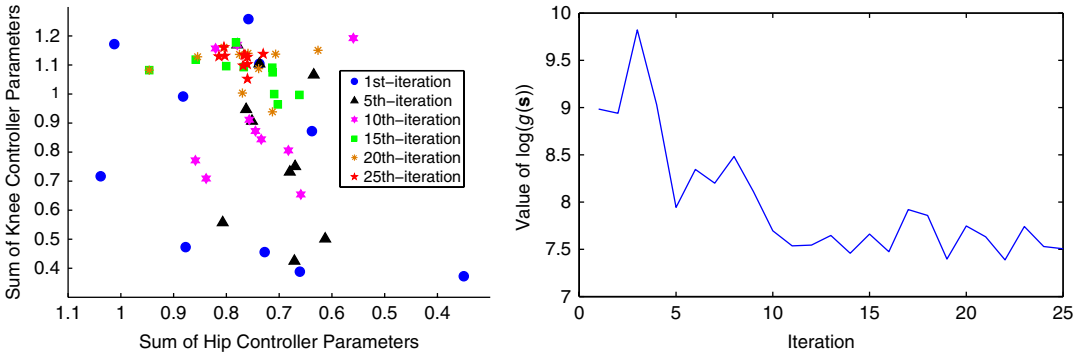


Fig. 10. The convergence procedure of the FA with the pre-defined object function and the best solution of each iteration.

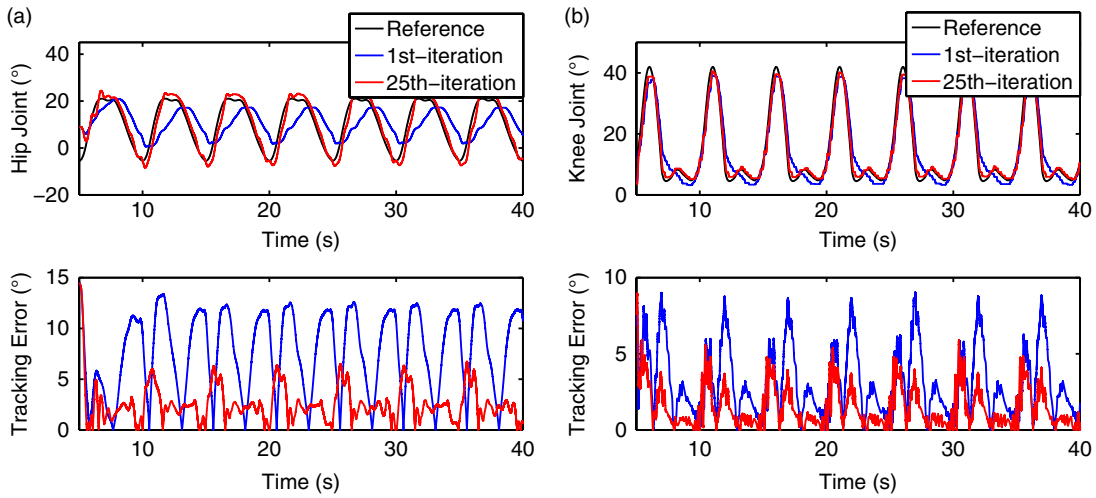


Fig. 11. The experimental studies of the proposed strategies with the mounted load, which is determined by the BSIPs. (a) Tracking performance of the hip joint based on the SMFA-PSMC. (b) Tracking performance of the knee joint based on the SMFA-PSMC.

lower limb. When conducting the experiments, the subjects were walking on the treadmill, and the weight support system was used to compensate the individual weight for simulating patients with weak lower limbs.

The results of the experiments on knee joint trajectory tracking with seven healthy volunteer subjects are presented in Fig. 12. All experiments were approved by the participants who have signed the Consent Form for prospective collection of medical information. It can be found that both the hip and knee joints can still get controlled to complete passive training tasks in the case of a large difference in the body weight of different people. It indicates the effectiveness of the control strategy for the exoskeleton, and this optimized control strategy shows a certain degree of robustness to weight.

https://doi.org/10.1017/S0263574719000511 Published online by Cambridge University Press

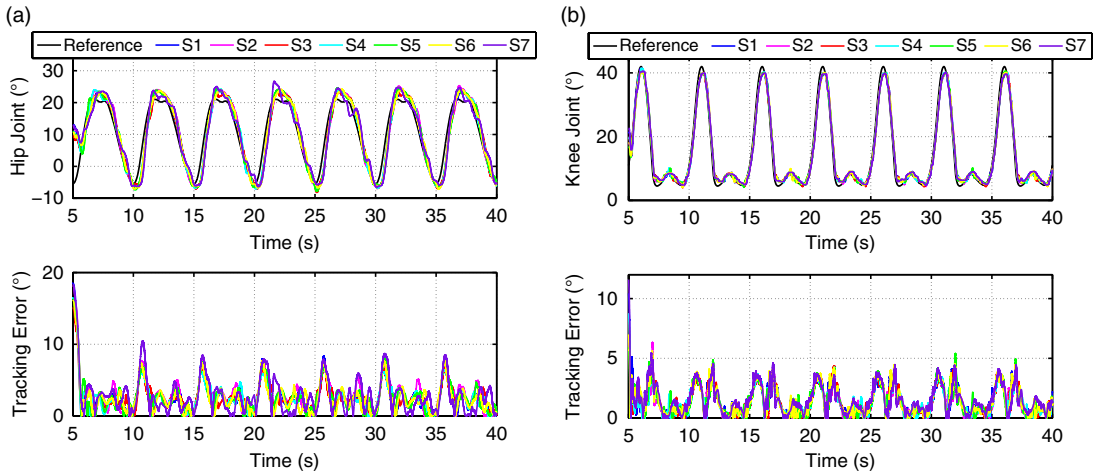


Fig. 12. Results of the experimental studies with four healthy subjects. (a) Results of the experiments on hip joint trajectory tracking with four healthy subjects. (b) Results of the experiments on knee joint trajectory tracking with four healthy subjects.

We use the Root Mean Square Error (RMSE) to measure the performance of the control strategy:

$$e_i = \sqrt{\frac{1}{2n}\sum_{t=1}^{n}(\theta_i(t) - \theta_{id}(t))^2}, (i = 1, 2), \tag{16}$$

where θ_1 and θ_2 are the real hip and knee joints angles. θ_{1d} and θ_{2d} are the corresponding reference trajectories. The tracking performance of the subjects' joints is measured with RMSE, as shown in Table III.

5.3. Discussion

The FA-based strategy can find global optima as well as all the local optima simultaneously. However, this requires a large population of fireflies, and it takes a lot of iterations. In this application, these factors are directly related to the time of learning. Therefore, we choose the upper and lower bounds of the control parameters and the appropriate population based on the simulation results to ensure that the fireflies can converge in a relatively short period. It is worth noting that the proportional gain k_p of PSMC may be very large in the simulation. Hence, we choose an appropriate range of k_p. Based on these considerations above, this strategy might not be guaranteed to find a global optimum, but it can still find a feasible sub-optimal solution that meets our requirement.

6. Conclusions

This paper presents a lower-limb exoskeleton that is actuated by the PMAs for rehabilitation. A mechanical mechanism of the exoskeleton system is designed to realize the wearing comfort for patients. Furthermore, due to the difficulties of modeling, we propose the SMFA-based PSMC to automatically calculate the pre-defined object function and attain the most applicable parameters for the specified rehabilitation task. Experimental studies are conducted and the results indicate the effectiveness of the proposed method.

Acknowledgments

This work was supported by the Beijing Advanced Innovation Center of Intelligent Robots and Systems under Grant (2016IRS10), the Research Fund of PLA of China (BWS17J024), the National Natural Science Foundation of China under Grant (61473130), the Graduate Innovation and Entrepreneurship Foundation of Huazhong University of Science and Technology under Grant (5003184017), and the Hubei Provincial Natural Science Foundation (Grant No. 2018CFB276)

https://doi.org/10.1017/S0263574719000511 Published online by Cambridge University Press

References

1. M. Dzahir and S. Yamamoto, "Recent trends in lower-limb robotic rehabilitation orthosis: Control scheme and strategy for pneumatic muscle actuated gait trainers," *Robotics* **3**(2), 120–148 (2014).
2. Z. Li, C. Y. Su, L. Wang, Z. Chen and T. Chai, "Nonlinear disturbance observer-based control design for a robotic exoskeleton incorporating fuzzy approximation," *IEEE Trans. Ind. Electron.* **62**(9), 5763–5775 (2015).
3. J. Huang, X. Tu and J. He, "Design and evaluation of the RUPERT wearable upper extremity exoskeleton robot for clinical and in-home therapies," *IEEE Trans. Syst. Man Cybern. Syst.* **46**(7), 926–935 (2016).
4. X. Li, Y. Pan, G. Chen and H. Yu, "Adaptive human-robot interaction control for robots driven by series elastic actuators," *IEEE Trans. Robot.* **33**(1), 169–182 (2017).
5. N. Paine, S. Oh and L. Sentis, "Design and control considerations for high-performance series elastic actuators," *IEEE/ASME Trans. Mechatron.* **19**(3), 1080–1091 (2014).
6. J. Zhang and P. Fiers, "Human-in-the-loop optimization of exoskeleton assistance during walking," *Science* **356**(6344), 1280–1284 (2017).
7. C. Jarrett and A. J. McDaid, "Robust control of a cable-driven soft exoskeleton joint for intrinsic human-robot interaction," *IEEE Trans. Neural Syst. Rehabil. Eng.* **25**(7), 976–986 (2017).
8. H. K. Yap, H. Y. Ng and C.-H. Yeow, "High-force soft printable pneumatics for soft robotic applications," *Soft Rob.* **3**(3), 144–158 (2016).
9. C. Teng, Z. Wong, W. Teh and Y. Z. Chong, "Design and Development of Inexpensive Pneumatically-Powered Assisted Knee-Ankle-Foot Orthosis for Gait Rehabilitation-Preliminary Finding," *International Conference on Biomedical Engineering (ICoBE)*, Penang, Malaysia (2012) pp. 28–32.
10. J. Cao, S. Q. Xie and R. Das, "MIMO sliding mode controller for gait exoskeleton driven by pneumatic muscles," *IEEE Trans. Control Syst. Technol.* **26**(1), 274–281 (2018).
11. W. James and H. Stuart, "Technical note: beyond the four-bar knee," *J. Prosthetics Orthotics* **10**(3), 77–80 (1998).
12. L. Zhu, X. Shi, Z. Chen, H. T. Zhang and C. H. Xiong, "Adaptive servomechanism of pneumatic muscle actuators with uncertainties," *IEEE Trans. Ind. Electron.* **64**(4), 3329–3337 (2017).
13. T. Karnjanaparichat and R. Pongvuthithum, "Adaptive tracking control of multi-link robots actuated by pneumatic muscles with additive disturbances," *Robotica* **35**(11), 2139–2156 (2017).
14. K. Xing, J. Huang, J. He, Y. Wang, J. Wu and Q. Xu, "Sliding mode tracking for actuators comprising pneumatic muscle and torsion spring," *Trans. Inst. Meas. Control* **34**(2–3), 255–277 (2012).
15. J. Wu, J. Huang, Y. Wang and K. Xing, "Nonlinear disturbance observer-based dynamic surface control for trajectory tracking of pneumatic muscle system," *IEEE Trans. Control Syst. Technol.* **22**(2), 440–455 (2014).
16. D. Zhang, X. Zhao and J. Han, "Active model-based control for pneumatic artificial muscle," *IEEE Trans. Ind. Electron.* **64**(2), 1686–1695 (2017).
17. Y. Yuan, Y. Yu and L. Guo, "Nonlinear active disturbance rejection control for the pneumatic muscle actuators with discrete-time measurements," *IEEE Trans. Ind. Electron.* **66**(3), 2044–2053 (2018).
18. G. Andrikopoulos, G. Nikolakopoulos and S. Manesis, "Advanced nonlinear PID-based antagonistic control for pneumatic muscle actuators," *IEEE Trans. Ind. Electron.* **61**(12), 6926–6937 (2014).
19. J. Huang, Y. Cao, C. Xiong and H.-T. Zhang, "An echo state Gaussian process based nonlinear model predictive control for pneumatic muscle actuators," *IEEE Trans. Autom. Sci. Eng.* 1–14 (2018). doi: 10.1109/TASE.2018.2867939.
20. J. Huang, J. Qian, L. Liu, Y. Wang, C. Xiong and S. Ri, "Echo state network based predictive control with particle swarm optimization for pneumatic muscle actuator," *J. Franklin Inst.* **353**(12), 2761–2782 (2016).
21. J. Huang, M. H. Ri, D. Wu and S. Ri, "Interval type-2 fuzzy logic modeling and control of a mobile two-wheeled inverted pendulum," *IEEE Trans. Fuzzy Syst.* **26**(4), 2030–2038 (2018).
22. R. Kikuuwe and H. Fujimoto, "Proxy-Based Sliding Mode Control for Accurate and Safe Position Control," *Proceedings of the 2005 IEEE International Conference on Robotics and Automation*, Orlando, USA (2006) pp. 26–31.
23. R. Kikuuwe, S. Yasukouchi, H. Fujimoto and M. Yamamoto, "Proxy-based sliding mode control: A safer extension of PID position control," *IEEE Trans. Rob.* **26**(4), 670–683 (2010).
24. G. Y. Gu, L. M. Zhu, C. Y. Su, H. Ding and S. Fatikow, "Proxy-based sliding-mode tracking control of piezoelectric-actuated nanopositioning stages," *IEEE/ASME Trans. Mechatron.* **20**(4), 1956–1965 (2015).
25. M. V. Damme, B. Vanderborght, B. Verrelst, R. V. Ham, F. Daerden and D. Lefeber, "Proxy-based sliding mode control of a planar pneumatic manipulator," *Int. J. Rob. Res.* **28**(2), 266–284 (2009).
26. P. J. Prieto, E. Rubio, L. Hernández and O. Urquijo, "Proxy-based sliding mode control on platform of 3 degree of freedom (3-DOF)," *Adv. Rob.* **27**(10), 773–784 (2013).
27. K. Deb, A. Pratap, S. Agarwal and T. Meyarivan, "A fast and elitist multiobjective genetic algorithm: NSGA-II," *IEEE Trans. Evol. Comput.* **6**(2), 182–197 (2002).
28. J. Kennedy and R. Eberhart, "Particle Swarm Optimization," *International Symposium on Neural Networks* (1995) pp. 1942–1948.
29. X. S. Yang, "Firefly Algorithms for Multimodal Optimization," *International Symposium on Stochastic Algorithms*, vol. 5792 (2009) pp. 169–178.
30. I. Fister, I. Fister Jr, X.-S. Yang and J. Brest, "A comprehensive review of firefly algorithms," *Swarm Evol. Comput.* **13**, 34–46 (2013).

https://doi.org/10.1017/S0263574719000511 Published online by Cambridge University Press

31. T. Niknam, R. Azizipanah-Abarghooee and A. Roosta, "Reserve constrained dynamic economic dispatch: A new fast self-adaptive modified firefly algorithm," *IEEE Syst. J.* **6**(4), 635–646 (2012).
32. M. H. Horng, "Vector quantization using the firefly algorithm for image compression," *Expert Syst. Appl.* **33**(1), 1078–1091 (2012).
33. K. A. Witte, A. M. Fatschel and S. H. Collins, "Design of a Lightweight, Tethered, Torque-Controlled Knee Exoskeleton," *2017 International Conference on Rehabilitation Robotics (ICORR)*, London, UK (2017) pp. 1646–1653.
34. G. E. P. Box and M. E. Muller, "A note on the generation of random normal deviates," *Ann. Math. Stat.* **2**(29), 610–611 (1958).
35. M. Crepinsek, S. H. Liu and M. Mernik, "Exploration and exploitation in evolutionary algorithms: A survey," *ACM Comput. Surv.* **45**(3), article 35 (2013).
36. X. S. Yang, *Nature-Inspired Metaheuristic Algorithms*, (Luniver Press, Beckington, UK, 2010).
37. S. Nadeau, D. Gravel, A. Arsenault and D. Bourbonnais, "Plantarflexor weakness as a limiting factor of gait speed in stroke subjects and the compensating role of hip flexors," *Clin. Biomech.* **14**(2), 125–135 (1999).
38. J. Jovic, A. Escande, K. Ayusawa, E. Yoshida, A. Kheddar and G. Venture, "Humanoid and human inertia parameter identification using hierarchical optimization," *IEEE Trans. Robot.* **32**(3), 726–735 (2016).
39. V. Zatsiorsky and V. Seluyanov, "The mass and inertia characteristics of the main segments of the human body," *Biomechanics* **VIII-B**, 1152–1159 (1983).
40. C. K. Cheng, "Segment inertial properties of Chinese adults determined from magnetic resonance imaging," *Clin. Biomech.* **15**, 559–566 (2000).
41. M. Rossi, A. Lyttle and B. Blanksby, "Body segment inertial parameters of elite swimmers using DXA and indirect methods," *J. Sport Sci. Med.* **12**(4), 761–775 (2013).

https://doi.org/10.1017/S0263574719000511 Published online by Cambridge University Press